Research Article

Dependence of ultrafast dynamics in gold–silver alloy nanoclusters on the proportion of the metal content

Soumyadip Bhunia[1] · **Sumit Kumar**[1] · **Pradipta Purkayastha**[1,2]

Abstract

Bimetallic nanoclusters (NCs) have attracted extensive attention in present research due to the synergic effect of the two kinds of metal atoms and their valuable applications. The broad range of applications of these noble metal NCs and their molecular nature instigated understanding their property of luminescence and the underlying ultrafast dynamics. With a view to enlighten the weakly known changes in excited state dynamics of luminescent noble metal alloy NCs, protein protected bimetallic alloy gold–silver NCs (Au–Ag NCs) with different molar ratios were synthesized and characterized. The results show that a particular optimum molar ratio of the two metal atoms gives maximum luminescence to the NCs. The findings from transient absorption spectroscopy and excited state decay analysis consolidated the results and provided detailed description in this direction. Various applications, such as optical energy harvesting, bio-medical imaging and photocatalysis, would find ample flexibility on knowing the characteristics of the alloy metal NCs that might lead to relevant modulations in their properties. The present study is intended to develop the concept of ultrafast dynamics in noble metal alloy NCs.

Graphical abstract Fluorescence intensity of gold–silver alloy nanoclusters is decided by an optimum molar ratio of the metals. One can synthetically impose maximum luminescence to the alloy nanoclusters knowing the underlying dynamics.

Electronic supplementary material The online version of this article (https://doi.org/10.1007/s42452-019-0473-9) contains supplementary material, which is available to authorized users.

✉ Pradipta Purkayastha, ppurkayastha@iiserkol.ac.in | [1]Department of Chemical Sciences, Indian Institute of Science Education and Research (IISER) Kolkata, Mohanpur, WB 741246, India. [2]Centre for Advanced Functional Materials (CAFM), Indian Institute of Science Education and Research (IISER) Kolkata, Mohanpur, WB 741246, India.

SN Applied Sciences (2019) 1:449 | https://doi.org/10.1007/s42452-019-0473-9

Received: 11 March 2019 / Accepted: 8 April 2019 / Published online: 11 April 2019

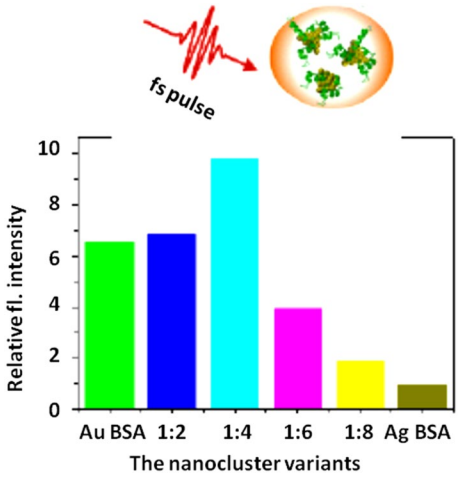

Keywords Bimetallic nanocluster · Fluorescence · Alloy · Transient absorption · Excited state dynamics · Molecular logic gate

1 Introduction

Noble metal nanoclusters (NCs) are typically constituted of a few tens of atoms [1, 2] that have extensive applications in the areas of biomarkers [3], optics [4], catalysis [5, 6] and sensors [7–10]. Existence of metal as atomic aggregates and hence their quantum confinement helps the metal NCs to exhibit "molecule-like" discrete electronic properties allowing optical tuning. This, characteristically, distinguish them from their nanoparticulate forms that typically show surface plasmon effects and do not emit radiatively. The metal NCs are generally composed of a metal core and a ligand shell with atomically precise core size [11, 12]. Understandably, the optical properties of the NCs are dominated by the core-derived states of the metal atoms and the binding shell [13, 14]. Techniques to characterize small molecules, such as, elemental analysis, UV/visible and IR spectroscopies, mass spectrometry, ^{1}H NMR, etc. can be suitably used to characterize the NCs [15].

Considering the broad range of applications of the noble metal NCs and their molecular nature, the property of luminescence and its understanding has become essentially important. A few works described these issues from the viewpoint of ligand-to-metal charge transfer (LMCT) and/or ligand-to-metal–metal charge transfer (LMMCT) [16, 17]. To enhance the photoluminescence, various research groups worked on modulating the surface functionalization of the NCs and protected them with polymers [18], thiols [19], and proteins [20, 21] and by doping the metal core with another suitable metal [22–26]. In a recent report, Negishi and co-workers differentially doped the gold (Au) core of thiolate protected NCs with silver (Ag) and discovered continuous modulation of the electronic structure of the thiolate protected Au NCs accompanied by change in the photoluminescence property [24]. On the other hand, pristine silver nanoclusters (Ag NCs) are reported to be brighter than the Au NCs [19, 27–29]. However, they are highly reactive and release Ag ions along with oxidation of Ag in solution and rapidly lose photoluminescence [30]. Based on the interesting properties of the doped Au and/or Ag NCs, they have been used in identifying toxic metals and applied for bioimaging and biosensing [31–36].

In the present context, we gave special attention to the mechanistic details of emission from the thiolate protected Au–Ag NCs that happens mainly through autofluorescence due to intraband transition [37]. Higher silver content produces a red shift in the optical spectral profile with an enhancement in emission intensity by 4 to 5 times on increasing the ratio of Ag in glutathione coated Au NCs (AuGSH) (excitation at 400 nm and emission at 615 nm) [23]. AuGSH and AuAgGSH show biexponential decay of fluorescence with a shorter and a longer lifetime components, where the longer component slows down due to redox processes on enhancement of the proportion of Ag in AuGSH [38, 39].

Till latest, glutathione (GSH) and thiolates were mostly used for the synthesis of strongly fluorescent Au–Ag bimetallic clusters. Only a few reports are there where such NCs were protected with protein [40–44]. It is pertinent that biocompatible Au–Ag NCs can be produced only by protecting them with naturally occurring biomolecules,

such as proteins, peptides and DNAs [45–47]. Protein-protected Au–Ag NCs conceptually resemble the naturally occurring metalloproteins, such as hemoglobin and superoxide dismutase [20]. Hence, we have revisited the problem to understand the details of the origin of emission from the Au–Ag NCs by synthesizing biocompatible clusters protected by bovine serum albumin (BSA) [48, 49]. Ultrafast spectroscopy showed that the fluorescence from the Au–Ag NCs does not increase gradually with increase in Ag concentration in Au NCs, but the maximum emission comes from an optimum ratio of Ag and Au (typically 1:4). Based on the observed facts on variation in the fluorescence quantum yield of these bimetallic NCs we have shown probable application in creating molecular logic gates.

2 Experimental

The chemical precursors, $HAuCl_4 \cdot 4H_2O$, $AgNO_3$, $NaBH_4$, NaOH, and BSA were purchased from Sigma-Aldrich and used as received without further purification. The solutions were prepared in triple distilled water. The absorption spectra were recorded in a Hitachi U-2900 spectrophotometer. The steady state fluorescence measurements were carried out using a QM 40 spectrofluorimeter from PTI Inc. The time-resolved fluorescence experiments were performed using a Horiba Jobin–Yvon Fluorocube instrument with a 377 nm diode laser excitation source (with a temporal resolution of 70 ps) using time correlated single photon counting (TCSPC) method. Electron dispersive spectroscopy (EDS) was performed using a JEM-2100F field emission gun electron microscope with EDS, diffraction pattern software, and high angle annular dark-field scanning transmission electron microscopy detector. Transmission electron microscopy (TEM) images were recorded with a JEOL, JEM-2100F microscope using a 200 kV electron source at the DST-FIST facility in IISER Kolkata. The dynamic light scattering (DLS) and the ξ-potential measurements were carried out in a Nano Particle Analyzer SZ-100 from Horiba Scientific. Thermogravimetric analysis (TGA) was done on a Mettler-Toledo TGA/SDTA 851e instrument. Approximately (5–6 mg) of the sample was added to an aluminium crucible and heated from 40 to 500 °C at a rate of 10 °C/min under continuous nitrogen purge. Powder X-ray diffraction was performed using a RIGAKU Smart Lab X-ray diffractometer using Cu Kα radiation operating at 35 kV and 70 mA.

Both pristine and alloy metal NCs were synthesized using reported protocols [45, 48, 49]. Synthesis of Au NCs was carried out at physiological temperature (37 °C). Upon adding $HAuCl_4$ to the aqueous BSA solution, the protein molecules sequestered Au ions and entrapped them. The pH of the solution was adjusted to 12 so that BSA could act as a reducing agent to produce the Au NCs in situ [45]. To synthesize the Ag NCs, a 5.0 mL aqueous solution of $AgNO_3$ (5.0 mM) was mixed with 5.0 mL of bovine serum albumin (BSA 96%, 60.0 mg/mL) in the dark at 0 °C under vigorous stirring. After 5 min, 20 µL of a freshly prepared aqueous solution of $NaBH_4$ (5 mM) was introduced to quickly reduce the Ag^+ ions. The solution of the mixture changed from colourless to pale brown after a few minutes. Stirring was continued to 4 h for sufficient generation of silver NCs [50]. The procedure has been represented in Scheme 1.

The bimetallic alloying Au–Ag NCs were prepared using BSA protein as the stabilizing and reducing agent using different molar ratios of $HAuCl_4$ and $AgNO_3$. An aliquot of $HAuCl_4$ solution (4.0 mL, 10 mM) was added to the BSA aqueous solution (5.0 mL, 50 mg/mL). Then, $AgNO_3$ solutions (1.0 mL) of different concentrations (~ 20.0, 10.0, 6.7 and 5.0 mM) were separately added under vigorous stirring for 10 min at 37 °C. Afterward, NaOH solution (1.0 mL, 1.0 M) was introduced immediately and incubated at 37 °C for 12 h. Finally, the resulting suspension was dialyzed in ultrapure water for 48 h with the water changed every 6 h to acquire gold–silver bimetallic nanoclusters (i.e., Au–Ag NCs) and stored at 4 °C for further use [48, 49]. The molecular weight cut-off (MWCO) for dialysis experiment was 6000–8000.

The experiments were performed in aqueous medium in solution phase. Concentration of the NCs was determined from the concentration of metal atom present in solution. A fixed volume of the aliquote was added each time to a constant volume of water for the experiments. The final concentration (360 µM) was calculated using (volume of aliquote)*(strength of aliquote) = (final volume)*(final strength). The samples were excited at 375 nm for the steady state spectral studies. The synthesized NCs were stored at 4 °C and there was practically no change in their characteristics for prolonged period of time. The protein coated red emitting NCs are generally very stable systems.

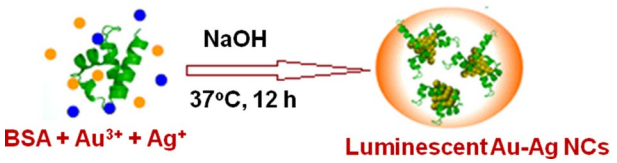

Scheme 1 Synthesis of BSA protected Au–Ag NCs

3 Results and discussion

BSA played a double role to act as a stabilizer and reducing agent for the synthesized Au–Ag NCs with different molar ratios of the respective metal precursors [48, 49]. The end products were obtained depending on the variation in the Ag^+ concentration in the Au NCs in solution phase. This was identified grossly by the colour differences as depicted in Fig. 1. The pristine Au and Ag NCs were of very small size (< 2 nm) as shown in the TEM images provided in Fig. 2. The bimetallic NCs were of similar size as depicted by the high resolution TEM (HR-TEM) images given in Fig. 2d (for 1:4 Ag:Au). The crystal structure of the obtained Au–Ag bimetallic NCs was characterized through XRD, as shown in Fig. S3. The obtained signals revealed that the sharp peaks at 31.92° and 45.89° could correspond to lattice planes (111) and (200) of the Au–Ag NCs, respectively proving the presence of both the metals in the alloy NCs. The XRD results were in agreement with previous reports [49]. DLS measurements provide that in aqueous medium the hydrodynamic diameters of the BSA protected Au and Ag NCs are ~ 5–6 nm and those for the alloy NCs are ~ 8–10 nm, respectively (Fig. S4).

Impact of the formation of the metal NCs on the secondary structure of BSA was monitored using circular dichroism (CD) spectroscopy. Figure 3a shows the CD spectrum of BSA and those for the respective

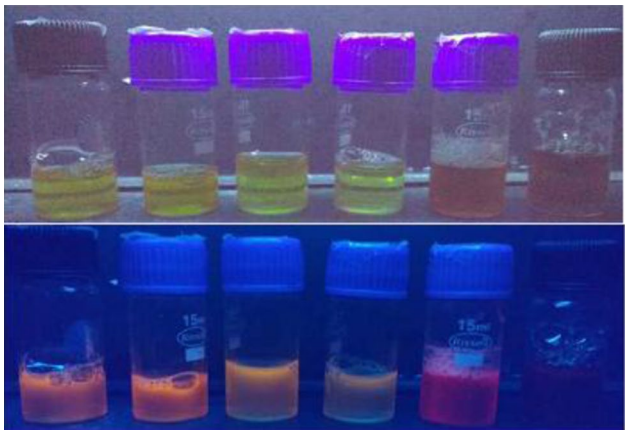

Fig. 1 Photographs of the Au–Ag NCs under normal (top panel) and UV (lower panel) lights. The Ag:Au ratios are 1:2,1:4,1:6,1:8 along with pristine Au and Ag NCs arranged from left to right

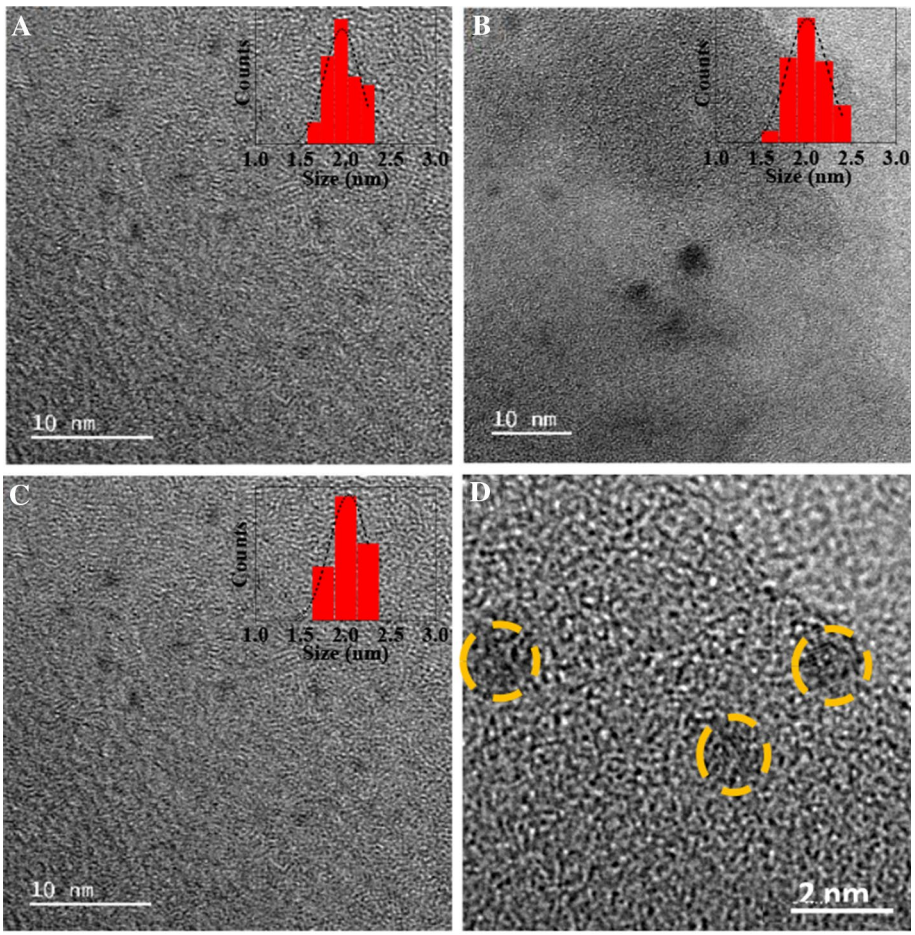

Fig. 2 TEM images of **a** Au NCs, **b** Ag NCs, **c** Au–Ag NCs mixed in 1:4 (Ag:Au) ratio and **d** HR-TEM image of Au–Ag NCs (Ag:Au 1:4). Some locations of in **d** have been circled for clarity

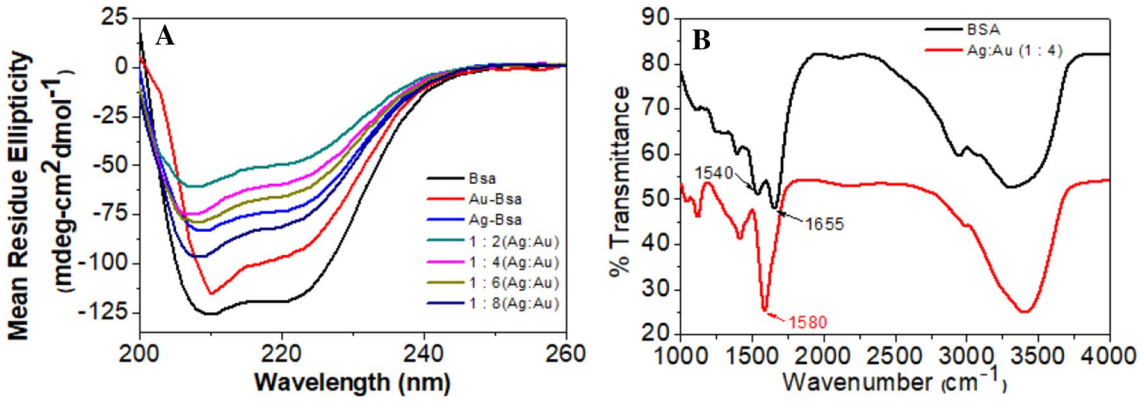

Fig. 3 CD spectra (**a**) and FTIR spectra (**b**) of BSA and BSA-protected pristine Au and Ag NC along with the alloy clusters

BSA-protected metal and alloy NCs. The CD spectrum of BSA is typically characterized by two negative bands at 208 nm and 222 nm, which are rationalized by the $n \rightarrow \pi^*$ transition [51], the so-called negative Cotton effect [52, 53], in the peptide bond of α-helix. The secondary conformation of BSA changes slightly on adding the NCs. A decrease in ellipticity indicates reduction in % α-helicity in BSA [54, 55]. However, the process does not completely destroy the folded structure of the protein but makes it partly unfolded. The FT-IR spectra of the species confirm changes in protein conformation on generating the BSA-protected Au–Ag bimetallic NCs. The characteristic amide I band at 1600–1700 cm^{-1} (primarily CO stretch) and amide II near 1545 cm^{-1} regions are the signature vibrational profiles for BSA (Fig. 3b). Broadening in the peak shape indicates formation of the NCs that, in turn, induces the secondary structural changes in BSA [48]. The ξ-potential data shows that the NCs have negative surface charge (Fig. S5). The TGA analysis provides stability of the NCs in terms temperature dependent weight loss which are almost similar (Fig. S6).

Characteristic featureless absorption spectra (Fig. 4a) suggest formation of stable Au and Au–Ag NCs [56]. In conventional noble metal nanoparticles, surface plasmon resonance dominates the optical response and shows strong quantum confinement effect with manifestations in the discrete UV–vis absorption spectrum [13]. Such a shoulder emerges for the pristine Ag NCs at 475 nm signifying nanopaticle nature (shown by an arrow in Fig. 4a) and hence relative instability. That is why, although Ag NCs are brighter than the Au NCs, their fluorescence quenches very quickly under normal conditions (Fig. 4b). Because of this inherent artefact of the Ag NCs, this work was not compared with Au-doped Ag NCs where the proportion of Ag is higher to Au.

The Au–Ag NCs show relative blue shift in their emission as the proportion of Ag decreases in the alloy NCs along with a concomitant reduction in fluorescence yield

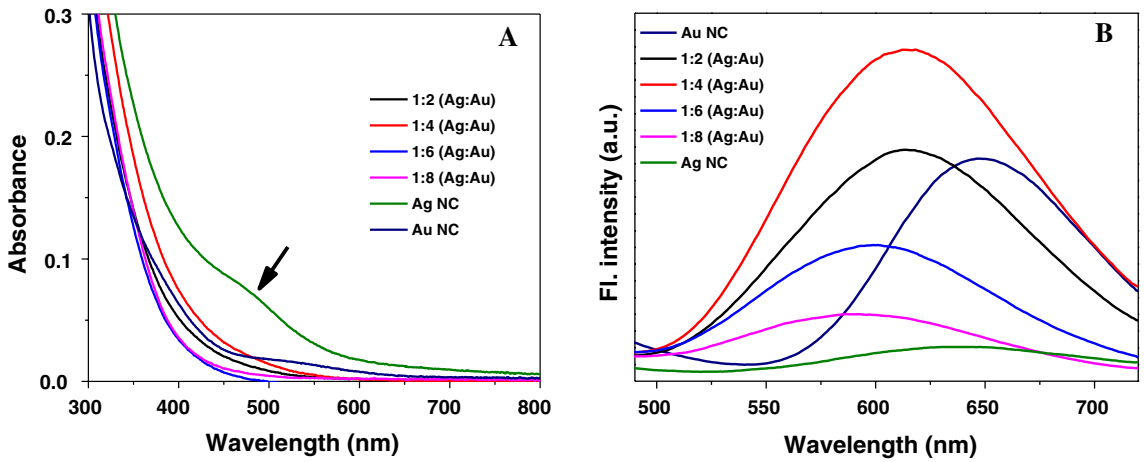

Fig. 4 **a** Absorption and **b** fluorescence spectra of pristine and alloy Au–Ag NC

(Fig. 4b). The 1:4 Ag–Au ratio in the alloy NCs shows highest fluorescence quantum yield which is even higher compared to the pristine Au NCs. The results indicate involvement of an optimal amount of Ag doping in Au NCs that is required to generate higher emission compared to the pristine metal NCs. Since the use of noble metal NCs is progressively increasing in the area of energy harvest, hence the mixing proportions of the metal atoms are necessary to be optimized to facilitate formulation of devices. Our attempt is to specify the optical properties of the optimally mixed Ag and Au atoms in the alloy NCs.

The fluorescence quantum yields (Q) were calculated for each of the species following the equation [57]:

$$Q = Q_R \frac{IA_R}{I_R A}\left(\frac{n}{n_R}\right)^2 \quad (1)$$

where, I (sample) and I_R (reference) are the integrated emission peak areas, A (sample) and A_R (reference) are the absorbances at the chosen wavelength, and n (sample) and n_R (reference) are the refractive indices of the solvents. The measurement was performed taking quinine sulphate (Q = 0.54) in 0.1 M H_2SO_4 as standard [58]. The calculated Q values for the various species are tabulated below (Table 1) [59]. Ag NCs are highly prone to oxidation that results into rapid decrease of fluorescence resulting to its unpopularity as a marker. The results show that this can be hugely averted by preparing the Au–Ag NCs [23].

The electronic states involved in the respective electron transitions and the optimal band gaps could be obtained by examining the respective excitation spectra of the metal NCs (Fig. 5). The pristine Au NCs show a shoulder at 335 and a band at 520 nm, whereas, for the alloy NCs although the shoulder at 335 nm still exists, the higher wavelength bands shifts to 445 nm. The low energy absorption band can be assigned to the $S_0 \rightarrow S_1$ transition, where S_0 and S_1 are the singlet ground and first excited states, respectively. The band shift occurs because of destabilization of the S_1 state due to the alloy formation. The shoulder at 335 nm is due to $S_0 \rightarrow S_n$ transition., where S_n indicates higher excited singlet states [60].

A complete insight into the excited state dynamics of the NCs could be obtained from the time resolved spectroscopic studies by scanning the electronic relaxation times. The fluorescence decay data of the pristine and the alloy NCs could be fitted by a three exponential function given by:

$$y = A_1 \exp\left(\frac{-t}{\tau_1}\right) + A_2 \exp\left(\frac{-t}{\tau_2}\right) + A_3 \exp\left(\frac{-t}{\tau_3}\right) \quad (2)$$

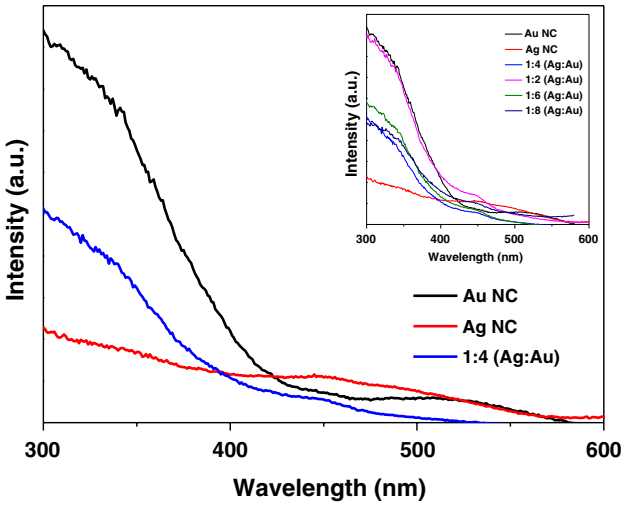

Fig. 5 Selected excitation spectra of the pristine and alloy Au–Ag NCs are shown for comparison. The spectra were obtained by monitoring the emission peaks. The inset shows excitation spectra for all the species

where τ_1, τ_2 and τ_3 represent the decay time constants, and A_1, A_2 and A_3 represent the respective amplitudes. Multiple components to the fit indicate the presence of more than one class of emitting species in the system as these are ligand (protein) assisted NC formation. As the nanoclusters are synthesized, the metal atoms (oxidation state 0) are protected by metal ions with +1 charge [45]. Because of this, electron transfer takes place between the species with 0 and + 1 oxidation states, which is termed as the inherent electron transfer. The emitting species, thus, are categorised into these three forms resulting multiple components [23]. Hence, it is customary to consider the average lifetime values (< τ >) to interpret the data following the equation:

$$\langle\tau\rangle = \frac{A_1\tau_1^2 + A_2\tau_2^2 + A_3\tau_3^2}{A_1\tau_1 + A_2\tau_2 + A_3\tau_3} \quad (3)$$

Table 2 provides the respective decay parameters of the emitting species along with the average lifetime values as obtained from the decay traces (Fig. S7). Each set of the data was fitted with a three exponential decay routine. τ_1 and τ_2 provide the decay times for the metal atoms in 0 and + 1 oxidation states, respectively [50]. The ultrafast decay time (τ_3) for the NCs is due to the inherent electron transfer. Pristine Ag NCs have extremely short average lifetime compared to the Au NCs and other alloy NCs.

Table 1 Relative fluorescence quantum yields of the various metal NCs

Species	Au NC	Ag NC	1:2 (Ag:Au)	1:4 (Ag:Au)	1:6 (Ag:Au)	1:8 (Ag:Au)
Quantum yields (%)	4.3	0.5	6.2	7.6	4.5	2.0

Table 2 Time resolved fluorescence decay parameters for pristine and alloy nanoclusters. The samples were excited at 377 nm and the emissions at 630 nm were monitored. The χ^2 values indicate the goodness of the respective fits

Sample	τ_1 (ps)	A_1 (%)	τ_2 (ns)	A_2 (%)	τ_3 (ns)	A_3 (%)	$<\tau>$ (ns)	χ^2
Au NC	318	5.43	4.33	3.95	182.54	90.62	182.34	1.05
Ag NC	385	29.45	2.21	41.60	7.32	28.96	5.58	1.12
1:2 (Ag:Au)	300	9.24	5.43	4.20	175.76	86.56	175.47	1.06
1:4 (Ag:Au)	236	11.51	4.59	3.05	180.59	85.44	180.40	1.02
1:6 (Ag:Au)	299	37.16	4.79	6.25	152.11	56.59	151.41	1.00
1:8 (Ag:Au)	286	33.03	5.13	9.24	149.41	57.73	148.46	1.07

This is because the lifetime components for Ag NCs are dominated by the fastest decaying species (~ 35 ps) and the fluorescence emission is lost quickly due to the synergistic effect [27, 48, 49]. On the other hand, for Au NCs and other alloy NCs, the second fastest component (~ 5 ns) could arise for the ligand (protein)-to-metal charge transfer (LMCT) transition influenced by solvent dependent emission phenomenon. The longer lifetime component (~ 150–200 ns) can be attributed to the HOMO to LUMO transition time of electron responsible for the red emission [61, 62]. The longer average lifetime value of 1:4 alloy NCs over the others signifies its better functionality.

The excited state behaviour of the various BSA-coated NCs was investigated using transient absorption spectroscopy (TAS) to analyse the time-dependent change in absorbance (ΔA) after exciting the sample with a 365 nm laser pulse (150 fs), energy density of 20 mW/cm^2 pulsed at 1 kHz). The samples were duly deaerated and placed in a 2 mm path length cuvette during the experiment. Figure 6 shows the excited state absorption (ESA) spectra and corresponding decay traces for the transient species absorbing at 535 nm at different delay times between 0.2 and 500 ps. The broad absorption spanning within the visible wavelengths represents the formation of the excited state species. In each of the cases, the raw data required two component fit dominated by the faster decaying species as shown in Table 3 [63, 64]. The decays at 535 nm indicate excited state HOMO to LUMO electron transfer processes occurring in the NCs. These fast processes occur quicker in the 1:4 alloys compared to the other species and hence loss in fluorescence due to the inherent excited state electron transfer is lesser. As a result the intensity of emission from the locally excited species is highest.

It has been reported earlier that the enhancement in the fluorescence quantum yield of the clusters depends on the nature of the excited state [22]. The number of Ag atoms in Au NCs affects the S_1 state significantly. Molecule-like efficient internal conversion (IC) (~ 1 ps) was observed before in Au NCs accompanied by core–shell charge transfer [65, 66]. Sfeir et al. attributed the faster decaying component to rapid IC [67]. The slower component in Table 2 was assigned to the fraction of the NCs that lives longer with delayed non-radiative processes, such as, IC or intersystem crossing (ISC) [56]. In the present case, on irradiation at 365 nm the electron may directly get transited to the higher excited singlet states (S_n) followed by faster decay in ~ 1–2 and 100 ps (Table 3). In the 1:4 Ag–Au NCs, the longest lifetime (Table 2) indicates less quenching of emission due to IC and/or ISC compared to the other alloys.

Careful analysis of the steady state fluorescence spectra reveals that while pristine Au and Ag NCs have a HOMO–LUMO band gap of ~ 1.9 eV, the alloys have it as ~ 2.0 eV. Precisely, the band gaps for the 1:2, 1:4, 1:6 and 1:8 Ag–Au alloys are 2.02, 2.02, 2.07 and 2.10 eV, respectively. Due to this variation in the band gap of the alloys, we observed blue shifts in the corresponding emission spectra compared to the pristine metal clusters. While 1:2 and 1:4 alloys have comparable band gaps, the other two are noticeably more. Difference in fluorescence quantum yield between the 1:2 and the 1:4 variants could be due to the presence of different ratios of Ag atoms in the Au NCs and hence modulating the extent of excited state electronic transitions.

The obtained results from the Au–Ag alloy NCs can be utilized to construct two simple molecular logic gate operations (Fig. 7). Considering the proportion of incorporated Ag^+ ions in the bimetallic NCs, YES and NOT logic gates could be built. As per previous reports, construction of various logic gates solely depends on external factors such as association and dissociation of sensing ions with or from a fluorophore and by alterations of pH and temperature of the environment [68–72]. On the contrary, here we have attempted to construct logic gates without influence of any such external factor. The percentage of Ag^+ ions present in bimetallic NCs was taken as input. The output was defined as 1 and 0 which corresponds to strong and weak fluorescence response. NOT and YES gates could be constructed in case of 1:8 and 1:4 bimetallic alloy NCs, respectively. In case of NOT gate, the fluorescence of Au-BSA is quenched by doping with lesser amount of Ag^+ ions (1:8 alloy) which indicating 0 output (low fluorescence). On the contrary, the fluorescence of Au-BSA is enhanced by doping with higher amount of Ag^+ ions compared to the previous instance (1:4 alloy) indicating output is 1 (strong fluorescence).

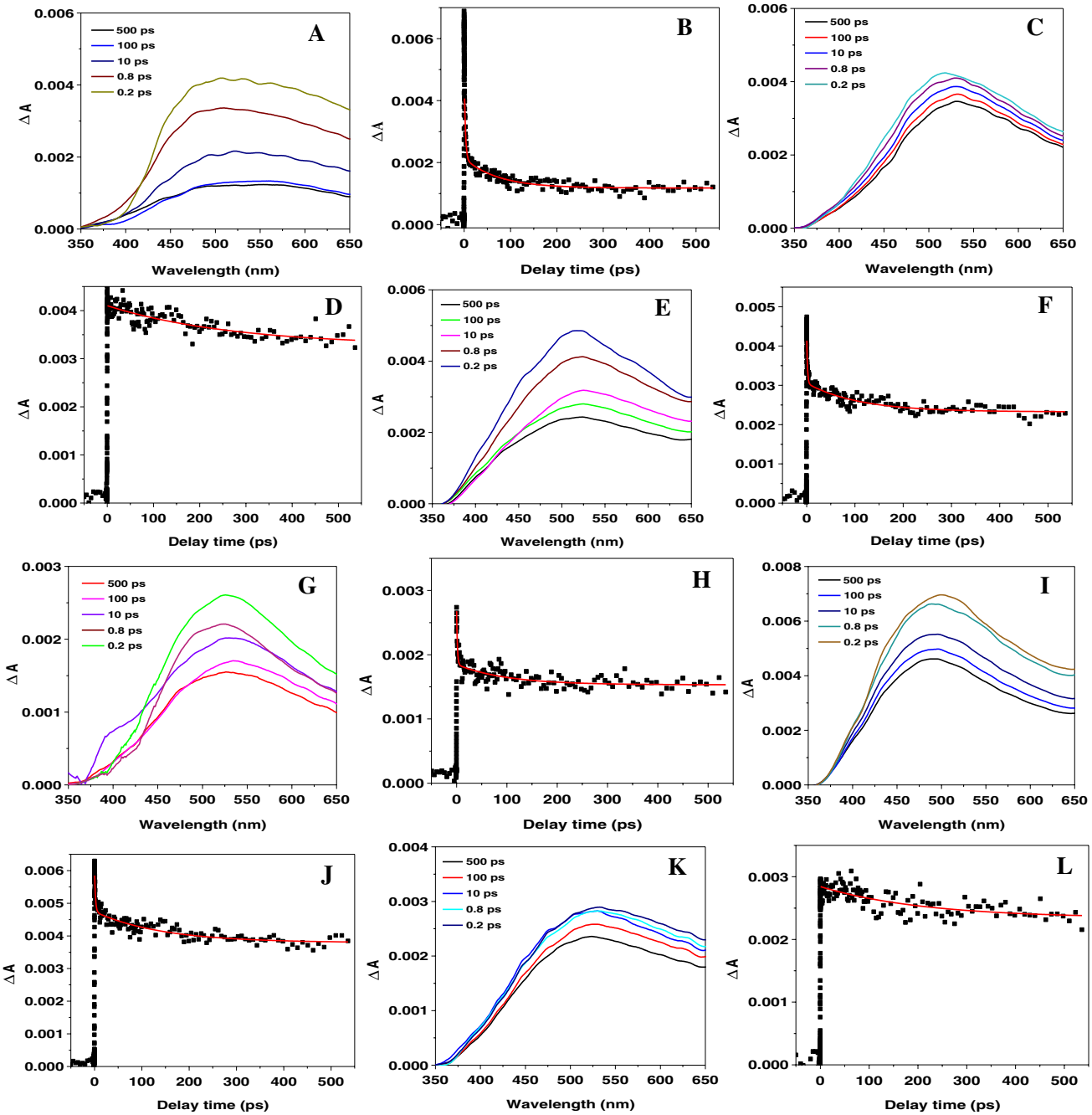

Fig. 6 Transient absorption (TA) spectra of BSA protected pristine and alloy (Au–Ag) NCs pumped over the 0.2–500 ps delay ranges: (**a**, **b**), (**c**, **d**), (**e**, **f**), (**g**, **h**), (**i**, **j**) and (**k**, **l**) are the respective spectra and kinetic decay profiles of Au NC, Ag NC, 1:2, 1:4, 1:6 and 1:8 (Ag:Au) alloy NCs. The decays were monitored at 535 nm

4 Conclusion

In conclusion, by revisiting the problem of excited state dynamics of BSA-protected Au–Ag NCs, we demonstrate that the NCs can emit variably and the quantum yield varies optimally considering the ratio of Ag in the Au NCs. It is found that 1:4 Ag:Au provides maximum fluorescence emission due to higher extent of electronic transition from the HOMO to LUMO. Although several reports are there on this topic using thiolate-protected Au–Ag NCs, however, hardly any conclusive description on the detailed photophysics of the alloy Au–Ag NCs are present. We could show that an optimum level of Ag-doping is needed to acquire maximum fluorescence from these alloys. The findings will help in establishing and extensively using the biologically non-toxic Au–Ag NCs as biomarkers.

Table 3 Kinetic data from TA spectral data for pristine and alloy NCs

Sample	τ_1 (ps)	% contribution	τ_2 (ps)	% contribution
Au NC	2.42	76	73.36	24
1:2 (Ag:Au)	1.54	66	107.82	34
1:4 (Ag:Au)	1.44	74	98.77	26
1:6 (Ag:Au)	1.97	58	143.00	42
1:8 (Ag:Au)	1.37	48	72.22	52

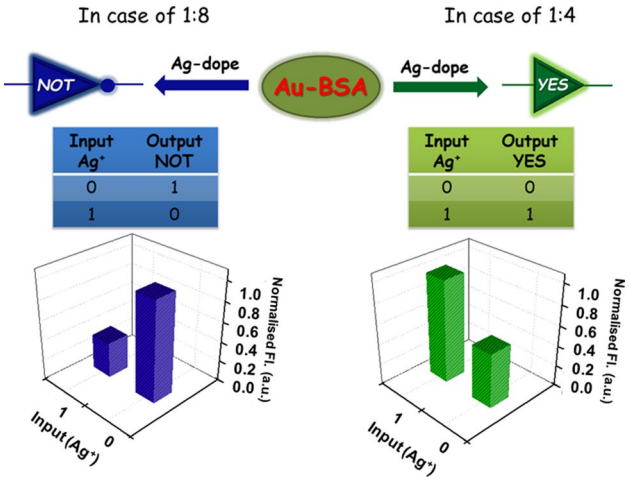

Fig. 7 Application of the variation of emission from the Au–Ag NCs in constructing molecular logic gates

Acknowledgements The work was supported by the Science and Engineering Research Board of the Department of Science and Technology, Government of India through the Project EMR/2015/000950. The authors are thankful to Dr. Suman Kalyan Pal of IIT Mandi for providing access to their transient absorption spectroscopy set-up and Dr. Dushyant Kushavah for helping in experiments. We acknowledge Dr. Somen Mondal for useful discussions. SB and SK acknowledge the Council of Scientific and Industrial Research and IISER Kolkata, respectively, for fellowships.

Funding This study was funded by Science and Engineering Research Board of the Department of Science and Technology, Government of India. (Grant Number EMR/2015/000950).

Compliance with ethical standards

Conflict of interest The authors declare that they have no conflict of interest.

References

1. Xavier PL, Chaudhari K, Baksi A, Pradeep T (2012) Protein-protected luminescent noble metal quantum clusters: an emerging trend in atomic cluster nanoscience. Nano Rev 3:14767
2. Zheng J, Nicovich PR, Dickson RM (2007) Highly fluorescent noble metal quantum dots. Annu Rev Phys Chem 58:409–431
3. Rosi NL, Giljohann DA, Thaxton CS, Lytton-Jean AKR, Han MS, Mirkin CA (2006) Oligonucleotide-modified gold nanoparticles for intracellular gene regulation. Science 312:1027–1030
4. Fan H, Yang K, Boye DM, Sigmon T, Malloy KJ, Xu H, López GP, Brinker CJ (2004) Self-assembly of ordered, robust, three-dimensional gold nanocrystal/silica arrays. Science 304:567–571
5. Zheng N, Stucky GD (2006) A general synthetic strategy for oxide-supported metal nanoparticle catalysts. J Am Chem Soc 128:14278–14280
6. Wan XK, Wang JQ, Nan ZA, Wang QM (2017) Ligand effects in catalysis by atomically precise gold nanoclusters. Sci Adv 3:e1701823
7. Wohltjen H, Snow AW (1998) Colloidal metal – insulator – metal ensemble chemiresistor sensor. Anal Chem 70:2856–2859
8. Govindaraju S, Ankireddy SR, Viswanath B, Kim J, Yun K (2017) Fluorescent gold nanoclusters for selective detection of dopamine in cerebrospinal fluid. Sci Rep 7:40298
9. Yu M, Zhu Z, Wang H, Li L, Fu F, Song Y, Song E (2017) Antibiotics mediated facile one-pot synthesis of gold nanoclusters as fluorescent sensor for ferric ions. Biosens Bioelectron 91:143–148
10. Madhuri UD, Radhakrishnan TP (2017) Gold nanoclusters with a wide range of fluorescence characteristics generated in situ in polymer thin films: potential gas sensing application. Dalton Trans 46:16236–16243
11. Jin R (2010) Quantum sized, thiolate-protected gold nanoclusters. Nanoscale 2:343–362
12. Purcell ST, Binh VT, Garcia N, Lin ME, Andres RP, Reifenberger R (1994) Field emission from narrow bands above the Fermi level of nanometer-scale objects. Phys Rev B 49:17259–17263
13. Zhu M, Aikens CM, Hollander FJ, Schatz GC, Jin R (2008) Correlating the crystal structure of a thiol-protected Au25 cluster and optical properties. J Am Chem Soc 130:5883–5885
14. Walter M, Akola J, Lopez-Acevedo O, Jadzinsky PD, Calero G, Ackerson CJ, Whetten RL, Grönbeck H, Häkkinen H (2008) A unified view of ligand-protected gold clusters as superatom complexes. Proc Natl Acad Sci USA 105:9157–9162
15. Udayabhaskararao T, Pradeep T (2013) New protocols for the synthesis of stable Ag and Au nanocluster molecules. J Phys Chem Lett 4:1553–1564
16. Chen Y, Yang T, Pan H, Yuan Y, Chen L, Liu M, Zhang K, Zhang S, Wu P, Xu J (2014) Photoemission mechanism of water-soluble silver nanoclusters: ligand-to-metal–metal charge transfer vs strong coupling between surface plasmon and emitters. J Am Chem Soc 136:1686–1689
17. Ishida H, Tobita S, Hasegawa Y, Katoh R, Nozaki K (2010) Recent advances in instrumentation for absolute emission quantum yield measurements. Coord Chem Rev 254:2449–2458
18. Santiago González B, Rodríguez MJ, Blanco C, Rivas J, López-Quintela MA, Martinho JMG (2010) One step synthesis of the smallest photoluminescent and paramagnetic PVP-protected gold atomic clusters. Nano Lett 10:4217–4221
19. Kumar S, Bolan MD, Bigioni TP (2010) Glutathione-stabilized magic-number silver cluster compounds. J Am Chem Soc 132:13141–13143
20. Luo Z, Zheng K, Xie J (2014) Engineering ultrasmall water-soluble gold and silver nanoclusters for biomedical applications. Chem Commun 50:5143–5155
21. Mathew A, Varghese E, Choudhury S, Pal SK, Pradeep T (2015) Efficient red luminescence from organic-soluble Au25 clusters by ligand structure modification. Nanoscale 7:14305–14315
22. Soldan G, Aljuhani MA, Bootharaju MS, AbdulHalim LG, Parida MR, Emwas A-H, Mohammed OF, Bakr OM (2016) Gold doping of silver nanoclusters: a 26-fold enhancement in the luminescence quantum yield. Angew Chem Int Ed 55:5749–5753

23. Bhunia S, Kumar S, Purkayastha P (2018) Gold nanocluster-grafted cyclodextrin suprastructures: formation of nanospheres to nanocubes with intriguing photophysics. ACS Omega 3:1492–1497
24. Negishi Y, Iwai T, Ide M (2010) Continuous modulation of electronic structure of stable thiolate-protected Au25 cluster by Ag doping. Chem Commun 46:4713–4715
25. Akutsu M, Koyasu K, Atobe J, Hosoya N, Miyajima K, Mitsui M, Nakajima A (2006) Experimental and theoretical characterization of aluminum-based binary superatoms of $Al_{12}x$ and their cluster salts. J Phys Chem A 110:12073–12076
26. Fields-Zinna CA, Crowe MC, Dass A, Weaver JEF, Murray RW (2009) Mass spectrometry of small bimetal monolayer-protected clusters. Langmuir 25:7704–7710
27. Udaya Bhaskara Rao T, Pradeep T (2010) Luminescent Ag_7 and Ag_8 clusters by interfacial synthesis. Angew Chem Int Ed 49:3925–3929
28. Richards CI, Choi S, Hsiang JC, Antoku Y, Vosch T, Bongiorno A, Tzeng YL, Dickson RM (2008) Oligonucleotide-stabilized Ag nanocluster fluorophores. J Am Chem Soc 130:5038–5039
29. Sharma J, Yeh HC, Yoo H, Werner JH, Martinez JS (2010) A complementary palette of fluorescent silver nanoclusters. Chem Commun 46:3280–3282
30. Wijnhoven SWP, Peijnenburg WJGM, Herberts CA, Hagens WI, Oomen AG, Heugens EHW, Roszek B, Bisschops J, Gosens I, Van de Meent D, Dekkers S, De Jong WH, Van Zijverden M, Sips AJAM, Geertsma RE (2009) Nano-Silver—a review of available data and knowledge gaps in human and environmental risk assessment. Nanotoxicology 3:109–138
31. Choi S, Dickson RM, Yu J (2012) Developing luminescent silver nanodots for biological applications. Chem Soc Rev 41:1867–1891
32. Guo W, Yuan J, Wang E (2009) Oligonucleotide-stabilized Ag nanoclusters as novel fluorescence probes for the highly selective and sensitive detection of the Hg^{2+} ion. Chem Commun. https://doi.org/10.1039/b821518a
33. Yu M, Zhou C, Liu J, Hankins JD, Zheng J (2011) Luminescent gold nanoparticles with pH-dependent membrane adsorption. J Am Chem Soc 133:11014–11017
34. Yuan X, Luo Z, Yu Y, Yao Q, Xie J (2013) Luminescent noble metal nanoclusters as an emerging optical probe for sensor development. Chem Asian J 8:858–871
35. Chevrier DM, Chatt A, Zhang P (2012) Properties and applications of protein-stabilized fluorescent gold nanoclusters: short review. J Nanophotonics 6:064504
36. Dou X, Yuan X, Yu Y, Luo Z, Yao Q, Leong DT, Xie J (2014) Lighting up thiolated Au@Ag nanoclusters via aggregation-induced emission. Nanoscale 6:157–161
37. Ristig S, Kozlova D, Meyer-Zaika W, Epple M (2014) An easy synthesis of autofluorescent alloyed silver–gold nanoparticles. J Mater Chem B 2:7887–7895
38. Patel SA, Cozzuol M, Hales JM, Richards CI, Sartin M, Hsiang JC, Vosch T, Perry JW, Dickson RM (2009) Electron transfer-induced blinking in Ag nanodot fluorescence. J Phys Chem C 113:20264–20270
39. Ganguly M, Mondal C, Pal J, Pal A, Negishi Y, Pal T (2014) Fluorescent Au(I)@Ag2/Ag3 giant cluster for selective sensing of mercury(II) ion. Dalton Trans 43:11557–11565
40. Taylor U, Tiedemann D, Rehbock C, Kues WA, Barcikowski S, Rath D (2015) Influence of gold, silver and gold-silver alloy nanoparticles on germ cell function and embryo development. Beilstein J Nanotechnol 6:651–664
41. Mohanty JS, Xavier PL, Chaudhari K, Bootharaju MS (2012) Luminescent, bimetallic AuAg alloy quantum clusters in protein templates. Nanoscale 4:4255–4262
42. Feng T, Chen Y, Feng B, Yan J, Di J (2019) Fluorescent red-shift of gold-silver nanoclusters upon interaction with cysteine and its application. Spectrochim Acta A 206:97–103
43. Zhou Q, Lin Y, Xu M, Gao Z, Yang H, Tang D (2016) Facile synthesis of enhanced fluorescent gold-silver bimetallic nanoclusters and its application for highly sensitive detection of inorganic pyrophosphatase activity. Anal Chem 88:8886–8892
44. Dai R, Deng W, Hu P, You C, Yang L, Jiang X, Xiong X, Huang K (2018) One-pot synthesis of bovine serum albumin protected gold/silver bimetallic nanoclusters for ratiometric and visual detection of mercury. Microchem J 139:1–8
45. Xie J, Zheng Y, Ying JY (2009) Protein-directed synthesis of highly fluorescent gold nanoclusters. J Am Chem Soc 131:888–889
46. Schaaff TG, Knight G, Shafigullin MN, Borkman RF, Whetten RL (1998) Isolation and selected properties of a 10.4 kDa gold:glutathione cluster compound. J Phys Chem B 102:10643–10646
47. Petty JT, Zheng J, Hud NV, Dickson RM (2004) DNA-templated Ag nanocluster formation. J Am Chem Soc 126:5207–5212
48. Zhou Q, Lin Y, Xu M, Gao Z, Yang H, Tang D (2016) Facile synthesis of enhanced fluorescent gold–silver bimetallic nanocluster and its application for highly sensitive detection of inorganic pyrophosphatase activity. Anal Chem 88:8886–8892
49. Zhang N, Si Y, Sun Z, Chen L, Li R, Qiao Y, Wang H (2014) Rapid, selective, and ultrasensitive fluorimetric analysis of mercury and copper levels in blood using bimetallic gold–silver nanoclusters with "silver effect"-enhanced red fluorescence. Anal Chem 86:11714–11721
50. Le Guével X, Hotzer B, Jung G, Hollemeyer K, Trouillet V, Schneider M (2011) Formation of fluorescent metal (Au, Ag) nanoclusters capped in bovine serum albumin followed by fluorescence and spectroscopy. J Phys Chem C 115:10955–10963
51. Yang P, Gao F (2002) The principle of bioinorganic chemistry. Science Press, Beijing, p 349
52. Greenfield N, Fasman GD (1969) Computed circular dichroism spectra for the evaluation of protein conformation. Biochemistry 8:4108–4116
53. Staprans I, Watanabe S (1970) Optical properties of troponin, tropomyosin, and relaxing protein of rabbit skeletal muscle. J Biol Chem 245:5962–5966
54. Xu H, Yao N, Xu H, Wang T, Li G, Li Z (2013) Characterization of the interaction between eupatorin and bovine serum albumin by spectroscopic and molecular modeling methods. Int J Mol Sci 14:14185–14203
55. Yu Y, Luo Z, Teo CS, Tan YN, Xie J (2013) Tailoring the protein conformation to synthesize different-sized gold nanoclusters. Chem Commun 49:9740–9742
56. Shi J, Cooper JK, Lindley S, Williams O, Kliger DS, Xu Y, Bao Y, Zhang JZ (2014) The excited state dynamics of protein-encapsulated Au nanoclusters. Chem Phys Lett 610–611:125–130
57. Lakowicz JR (2006) Principles of Fluorescence Spectroscopy, 3rd edn. Springer, Berlin
58. Fletcher AN (1969) Quinine sulfate as a fluorescence quantum yield standard. Photochem Photobiol 9:439–444
59. Zhang J, Yuan Y, Wang Y, Sun F, Liang G, Jiang Z, Yu S-H (2015) Microwave-assisted synthesis of photoluminescent glutathione-capped Au/Ag nanoclusters: a unique sensor-on-a-nanoparticle for metal ions, anions, and small molecules. Nano Res 8:2329–2339
60. Wen XM, Yu P, Toh YR, Hsu AC, Lee YC, Tang J (2012) Fluorescence dynamics in BSA-protected Au25 nanoclusters. J Phys Chem C 116:19032–19038
61. Mishra D, Aldeek F, Lochner E, Palui G, Zeng B, Mackowski S, Mattoussi H (2016) Aqueous growth of gold clusters with tunable fluorescence using photochemically modified lipoic acid-based ligands. Langmuir 32:6445–6458

62. Baral A, Basu K, Ghosh S, Bhattacharyya K, Roy S, Datta A, Banerjee A (2017) Size specific emission in peptide capped gold quantum clusters with tunable photoswitching behavior. Nanoscale 9:4419–4429
63. Yau SH, Varnavski O, Goodson T (2013) An ultrafast look at Au nanoclusters. Acc Chem Res 46:1506–1516
64. Qian H, Sfeir MY, Jin R (2010) Ultrafast relaxation dynamics of $[Au_{25}(SR)_{18}]_q$ nanoclusters: effects of charge state. J Phys Chem C 114:19935–19940
65. Devadas MS, Kim J, Sinn E, Lee D, Goodson T, Ramakrishna G (2010) Unique ultrafast visible luminescence in monolayer-protected Au_{25} Clusters. J Phys Chem C 114:22417–22423
66. Devadas MS, Thanthirige VD, Bairu S, Sinn E, Ramakrishna G (2013) Temperature-dependent absorption and ultrafast luminescence dynamics of bi-icosahedral Au_{25} clusters. J Phys Chem C 117:23155–23161
67. Sfeir MY, Qian H, Nobusada K, Jin R (2011) Ultrafast relaxation dynamics of rod-shaped 25-atom gold nanoclusters. J Phys Chem C 115:6200–6207
68. Dhenadhayalan N, Lin KC (2015) Chemically induced fluorescence switching of carbon-dots and its multiple logic gate implementation. Sci Rep 5:10012
69. Bandi R, Devulapalli NP, Dadigala R, Gangapuram BR, Guttena V (2018) Facile conversion of toxic cigarette butts to n, s-codoped carbon dots and their application in fluorescent film, security ink, bioimaging, sensing and logic gate operation. ACS Omega 3:13454–13466
70. Huang Z, Wang M, Guo Z, Wang H, Dong H, Yang W (2018) Aggregation-enhanced emission of gold nanoclusters induced by serum albumin and its application to protein detection and fabrication of molecular logic gates. ACS Omega 3:12763–12769
71. Lin X, Liu Y, Deng J, Lyu Y, Qian P, Li Y, Wang S (2018) Multiple advanced logic gates made of DNA-Ag nanocluster and the application for intelligent detection of pathogenic bacterial genes. Chem Sci 9:1774–1781
72. Zhang J, Chen C, Xu X, Wang X, Yang X (2013) Use of fluorescent gold nanoclusters for the construction of a NAND logic gate for nitrite. Chem Commun 49:2691–2693